AD-A180 159 INTERPRETATION OF X-RAY SPECTRA FROM NEON PLASMAS PRODUCED BY GAS IMPLOSIONS(U) SACHS/FREEMAN ASSOCIATES INC LANDOVER MD G MEHLMAN ET AL 23 MAR 87 NRL-MR-5956 1/1

UNCLASSIFIED F/G 20/9 NL

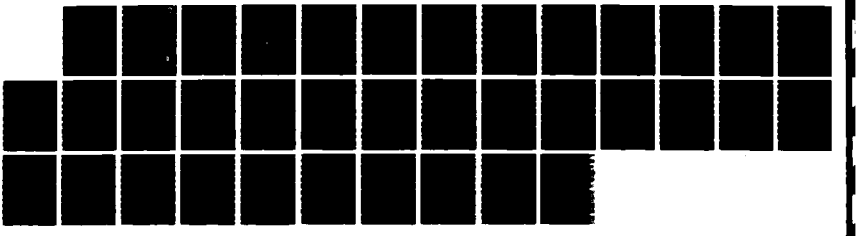

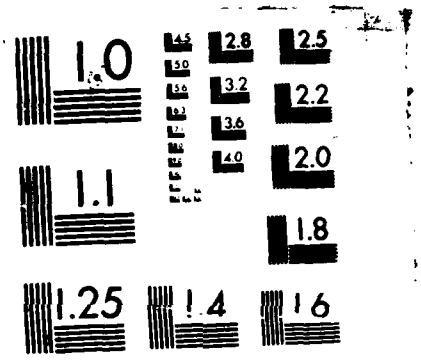

Naval Research Laboratory

Washington, DC 20375-5000

NRL Memorandum Report 5956

Interpretation of X-Ray Spectra from Neon Plasmas Produced by Gas Implosions

G. MEHLMAN,* P. G. BURKHALTER, AND D. A. NEWMAN*

Condensed Matter Physics Branch
Condensed Matter and Radiation Sciences Division

**Sachs/Freeman Associates, Inc.*

March 23, 1987

SECURITY CLASSIFICATION OF THIS PAGE

REPORT DOCUMENTATION PAGE

1a REPORT SECURITY CLASSIFICATION UNCLASSIFIED	1b RESTRICTIVE MARKINGS
2a SECURITY CLASSIFICATION AUTHORITY	3 DISTRIBUTION/AVAILABILITY OF REPORT Approved for public release; distribution unlimited.
2b DECLASSIFICATION/DOWNGRADING SCHEDULE	
4 PERFORMING ORGANIZATION REPORT NUMBER(S) NRL Memorandum Report 5956	5 MONITORING ORGANIZATION REPORT NUMBER(S)
6a NAME OF PERFORMING ORGANIZATION Naval Research Laboratory 6b OFFICE SYMBOL (If applicable) Code 4680	7a NAME OF MONITORING ORGANIZATION
6c ADDRESS (City, State, and ZIP Code) Washington, DC 20375-5000	7b ADDRESS (City, State, and ZIP Code)
8a NAME OF FUNDING/SPONSORING ORGANIZATION Defense Nuclear Agency 8b OFFICE SYMBOL (If applicable)	9 PROCUREMENT INSTRUMENT IDENTIFICATION NUMBER
8c ADDRESS (City, State, and ZIP Code) Washington, DC 20305-1000	10 SOURCE OF FUNDING NUMBERS PROGRAM ELEMENT NO: 62715H PROJECT NO: T99 QMXLA TASK NO: WORK UNIT ACCESSION NO:

11 TITLE (Include Security Classification)
Interpretation of X-Ray Spectra from Neon Plasmas Produced by Gas Implosions

12 PERSONAL AUTHOR(S)
Mehlman,* G., Burkhalter, P. G., and Newman,* D. A.

13a TYPE OF REPORT	13b TIME COVERED	14 DATE OF REPORT (Year, Month, Day)	15 PAGE COUNT
Memorandum	FROM _____ TO _____	1987 March 23	36

16 SUPPLEMENTARY NOTATION
*Sachs/Freeman Associates, Inc.

17 COSATI CODES			18 SUBJECT TERMS (Continue on reverse if necessary and identify by block number)
FIELD	GROUP	SUB-GROUP	Neon implosions X-ray spectroscopy Plasma parameters

19 ABSTRACT (Continue on reverse if necessary and identify by block number)

Spectroscopic measurements of imploded neon plasmas in the energy range 900-1600 eV provide estimates of the plasma thermodynamic properties. Plasma temperatures are found to be in the range 100-140 eV. There is experimental evidence for electron densities of several times 10^{21} cm^{-3}. Temperature and density gradients are discussed especially for the case of plasmas generated without a fast risetime current driving the implosion. Plasma dynamic properties such as dimensions of the emitting volume for the observed ion radiation and ionic velocities are discussed, based on the spectral line widths.

20 DISTRIBUTION/AVAILABILITY OF ABSTRACT	21 ABSTRACT SECURITY CLASSIFICATION	
☐ UNCLASSIFIED/UNLIMITED ☒ SAME AS RPT ☐ DTIC USERS	UNCLASSIFIED	
22a NAME OF RESPONSIBLE INDIVIDUAL P. G. Burkhalter	22b TELEPHONE (Include Area Code) (202) 767-2154	22c OFFICE SYMBOL Code 4681

DD FORM 1473, 84 MAR 83 APR edition may be used until exhausted. All other editions are obsolete.

SECURITY CLASSIFICATION OF THIS PAGE

U.S. Government Printing Office: 1985-607-047

CONTENTS

INTERPRETATION OF X-RAY SPECTRA FROM NEON PLASMAS PRODUCED BY GAS IMPLOSIONS

I. INTRODUCTION

Spatially-resolved x-ray spectra were collected for neon plasmas produced by imploding hollow annular gas puffs with the Gamble II pulsed power generator. Absolute emissivity values were obtained for the radiation emitted in the Ne IX and Ne X discrete transitions as well as for the total x-ray emission over the spectral range, 900-1600 eV. The analyzed spectra correspond to two different risetime driving currents produced with or without the adjunction of a plasma erosion opening switch (PEOS) between the generator and the gas puff. Details of the experimental arrangement, data analysis and results with tabulated values of the spectral energies and line widths have been reported (1).

Neon K-shell discrete transitions consist of the np—1s series of Ne IX (helium-like) and Ne X (hydrogen-like) ions. The first lines of each ion main series are listed in Table I together with some basic atomic parameters. The line wavelengths for Ne X are taken from the computation of Garcia and Mack (2) while the energy levels of Ne IX are extracted from the tables of Ermolaev and Jones (3) which are based on refined calculations of two-electron ion states. The radiative probabilities, A, and oscillator strengths, f, were computed using the atomic structure code provided by Cowan (4) although the hydrogenic values are obtained straightforwardly.

The interpretation of our spectra is based, on one hand, on derivations from line or continuum intensity measurements and, on the other hand, on the conclusions from line profile observations. In Section II, the plasma electron temperature is inferred from line ratios, and electron density estimates are derived from the measured lowering of the ionization threshold in the spectra. In Section III, we indicate a range of values for the

Manuscript approved December 16, 1986.

Table 1

Ne IX and Ne X Transitions

		Ne IX		$1s^2$—1snp series	
n		λÅ	E_{eV}	A x 10^{12} s^{-1}	f
2	He-α	13.447	922	9.16	0.75
	intercomb.	.55		0.0043	0.3004
3	He-β	11.547	1074	2.62	0.16
4	He-γ	11.000	1127	1.10	0.06
5	He-δ	10.76	1151	0.57	0.03
6		10.64	1164	0.337	0.017
7		10.56	1173	0.22	0.011

		Ne X		1s-np series	I.P. 1362.1 eV
n		λÅ	E_{eV}	A x 10^{12} s^{-1}	f
2	L-α	12.134	1022	6.265	0.416
3	L-β	10.239	1211	1.672	0.079
4	L-γ	9.708	1277	0.6818	0.032
5		9.481	1308	0.3437	0.016
6		9.362	1324	0.197	0.0093
7		9.291	1334	0.125	0.0059

implosion diameter, and for ion velocities during the x-ray radiation phase of the implosion, thereby, accounting for broad line profiles observed in the spectra. Section IV is devoted to relative ionic population considerations based on the absolute line intensity measurements. These results are summarized in Section V.

II. NEON PLASMA THERMODYNAMIC PARAMETERS: TEMPERATURE AND DENSITY

A. Temperature Estimates

In this section the plasma electron temperature is derived from temperature-dependent theoretical line ratios equated to the observed ratios. The latter are measured from spectral traces, such as the one presented in Fig. 1, where the energy radiated in a given discrete transition is obtained directly from the computed intensity values summed over the line profile. Details for this derivation are given in Ref. 1. The trace shown in Fig. 1 corresponds to a neon implosion generated without the switch. The intensity is on a log scale to emphasize the weaker portions of the spectrum.

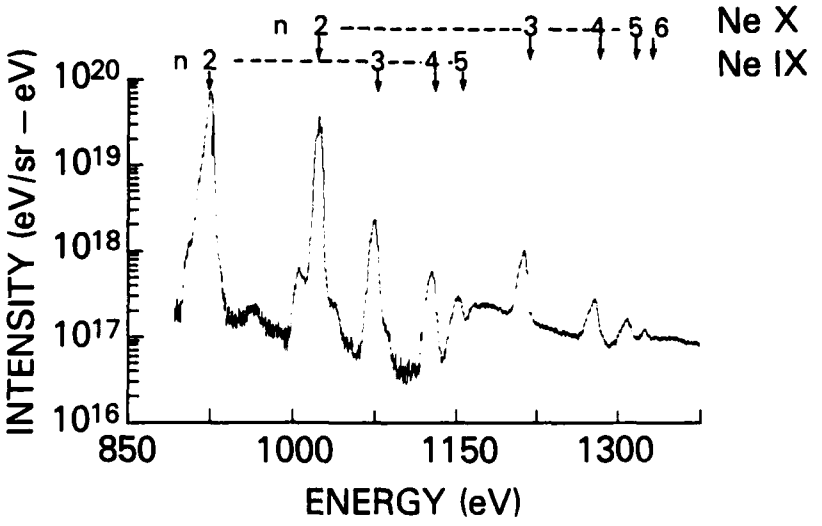

Figure 1. Intensity traces with Ne IX and Ne X lines

To calculate a discrete line intensity, one confronts the problem of describing the distribution of the ions among the various stages of ionization in abundance and, among the various excited levels of each ion. Various plasma ionization models are commonly used (5) with accepted criteria of applicability. We shall restrict ourselves here, to a few line intensity predictions using different ionization equilibria according to the pair of excited levels involved in the ratio. In the three cases considered below the corresponding assumptions will be justified. In all cases, the predictions will be made assuming a large probability of escape through the plasma for the photons, i.e., in the so-called optically thin approximation. In the section on line profiles, we shall give a justification for this procedure in a high density plasma ($>10^{18}$ cm^{-3}). Finally, since only steady-state solutions will be considered for simplicity, we shall discuss briefly the validity of the ionization models for imploding plasmas where electron temperature and/or density variations may take place at too fast a rate relative to the relaxation rates of the dominant atomic processes.

(1) Thermodynamic equilibrium

Two discrete levels n, n' (n<n') can be considered to be in thermal equilibrium if the electronic density, N_e, in the plasma reaches the value (6):

$$N_e \geq 1.7\ 10^{14}\sqrt{T_e}\cdot(\Delta E_{n,n'})^3$$

for N_e in cm^{-3}, and plasma temperature, T_e, and energy level difference, $\Delta E_{n,n'}$, in eV. For all the levels of Ne IX and Ne X ions with $n > 2$, $\Delta E_{nn'} \leq 66$ eV so, for an "equilibrium" $T_e < 200$ eV, we can assume Boltzmann populations in the neon plasma except for the ground state and the n=2 states provided:

$$N_e \geq 7.10^{20}$$

These conditions are usually met everywhere in the imploded neon plasmas. We note that the n=2 levels would achieve Boltzmann populations for electronic densities in excess of 10^{22} cm^{-3}, which could be attained on axis at the end of the time of full implosion (see below).

(2) Collisionally-dominated equilibrium

It is reasonable to consider that the n=2 levels are mainly populated by electron-collisional excitation from the ground state. This so-called "coronal limit" equilibrium is valid for electron densities smaller than N_e^* with:

$$N_e^* = \frac{\sum_{j<n} A_{nj}}{\langle \sigma_{n-1} \cdot v \rangle}$$

with: j lower state, n excited state, A_{nj} radiative probability, $\langle \sigma_{n-1} \cdot v \rangle$ collisional deexcitation rate from level n to ground state in cm^3/s. For the Ne IX and Ne X transitions we find the condition $N_e \ll N_e^*$ is always fulfilled for n=2 and n=3 as long as Te $\leq$ 140 eV.

With this model the line intensity (α and β transitions) is simply:

$$I_{n-1} = h\nu \cdot N_e \cdot n_i \langle \sigma_{1-n} \cdot v \rangle \cdot \frac{A_{n-1}}{\sum_j A_{nj}} \qquad (1)$$

the last factor being ~1 for the α (n=2) transitions. For the collisional excitation rate values $\langle \sigma_{1-n} \cdot v \rangle$ we used the parametric derivation of Sobelman, et al. (Ref. 5 p 212) in the Coulomb-Born approximation. N_e is the electron density (cm^{-3}) and n_i is the number of ions in the ground state. The line intensity is expressed in the same units as the transition energy ($h\nu$) per second.

This "coronal" approximation is reasonable to predict the α line intensities, for small optical depths in these transitions. Even if this were not

realistic for our high density plasmas, we restrict our line ratio derivation in this limit to the α line ratio, $R = \frac{I(He\text{-}\alpha)}{I(L\text{-}\alpha)}$, for which the opacity effect should be of comparable magnitude for both transitions with oscillator strengths differing by less than a factor of 2 (f values in Table I).

At this point we stress the influence of a temperature difference between the emitting ions, on the predicted α line ratio R. In the absence of time-resolved data for the different ion lines we rely on our line ratio observations (see (4)) to support the assumption of different regions in the plasma corresponding to each ion maximum radiation. However, this plasma model seems realistic for a fast-moving implosion-generated plasma where the population density rates of change depend on the electron density and temperature time-

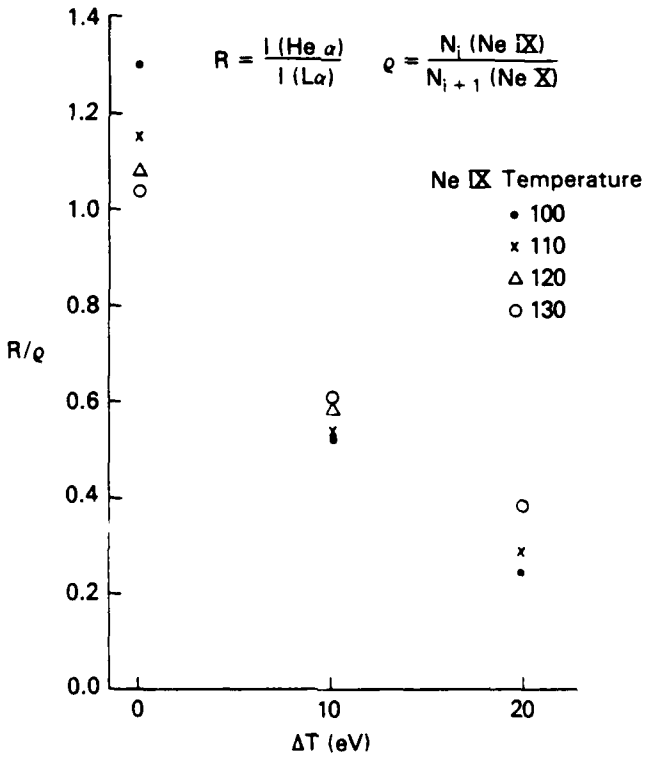

Figure 2. Effect of a temperature difference on the predicted line intensity ratio of the α-lines in Ne IX and X ions. $\Delta T = T_{Ne\ X} - T_{Ne\ IX}$.

evolution during the radiation. The collisional excitation rates $\langle\sigma_{1\text{-}2}\cdot v\rangle$ were calculated for several temperatures in the range 100 - 130 eV and the ratio R derived for a temperature difference ΔT between the Ne IX and Ne X ions of 0, 10 and 20 eV. The electronic density was considered constant in all emitting regions. Calling ρ the ion relative population, $\rho = \frac{N_i(\text{Ne IX})}{N_{i+1}(\text{Ne X})}$, we plot the value of $\frac{R}{\rho}$ versus ΔT in Fig. 2. The temperature in this figure is the lower one ascribed to the Ne IX ion region (or emission time). Clearly the predicted line ratio takes into account only one temperature-dependent factor, the collisional excitation rates, while associating each ion population to each region. This procedure is justified only because of the much larger Ne IX population (see in IV Table VI) allowing to disregard this ion contribution from the higher temperature zone.

(3) Collisional-radiative equilibrium for 2p and 3d levels of Ne X

A striking characteristic of the collisional excitation rates of hydrogen-like ions is the much larger magnitude of the 2p to 3d rate compared to the other rates (5) for plasma temperatures in the range 100-200 eV. This allows a simple description of the steady-state population distribution between the n=2 and n=3 levels of Ne X. Neglecting ionization and recombination rates, we may include simply 2p-3d collisional excitation and de-excitation processes and radiative decays. We obtain for the α to β line ratio:

$$\frac{I_\alpha}{I_\beta} = R_{LTE}(1+\gamma)$$

where the factor γ represents departure from local-thermodynamic equilibrium (LTE). For Ne X: $R_{LTE} = 3.165\ e^{\frac{189}{T}}$ (T in eV) and:

$$\gamma = \frac{7.8\text{x}10^{-2}}{k} \cdot \frac{\sqrt{T}\ (189 + 0.418\ T)}{189 + T} .$$

We have used excitation rate parameters from Ref. 5; the electron density is expressed as k x 10^{21} cm^{-3}; and the plasma electron temperature, T, is in eV.

Table II gives predicted line ratios for $\frac{2p\text{-}1s}{3p\text{-}1s}$ transitions of Ne X with this model. These ratios were evaluated in the temperature range, 100 to 150 eV, and the density range, 10^{21} (coronal limit) to 10^{22} (~LTE) per cm^3 (i.e., $1 \leq k \leq 10$). The coronal limit (k=1) values were obtained for collisional excitation processes 1s-3p which become predominant for $k \leq 1$.

Table II Predicted line intensity ratios, $\frac{I(L\text{-}\alpha)}{I(L\text{-}\beta)}$, for Ne X

	T_e eV	100	110	120	130	140	150
k	>10 → LTE	21	18	15	13.5	12	11
	10	22	19	16	14	13	12
	5		20	17	15	14	12.5
	3		25	18	16.5	15	13.5
	1→coronal		27	23	21	19	17

(4) Plasma temperature determinations

We have measured the line intensity ratios for the transitions $\frac{3p\text{-}1s}{4p\text{-}1s}$ (β transitions) for both ions Ne IX and Ne X. For the Ne IX line ratios (Heβ/Heγ), the measured values, averaged over several shots, are 3.5-4.0, corresponding to a temperature of 80-115 eV assuming that the excited levels (ΔE = 53 eV) are in thermodynamic equilibrium. The same line ratio for the Ne X ions varies from 3.6 to 4.0, corresponding to 100-150 eV for Ne X ions (assuming LTE for the upper levels).

The line ratio for higher Rydberg members, such as γ/δ (transitions $\frac{4p\text{-}1s}{5p\text{-}1s}$), is determined with larger experimental uncertainty due to the weaker line intensities over background. At the same time, the ratio becomes less temperature sensitive (in our plasma temperature range) due to the smaller upper level energy difference (24 and 31 eV respectively for the γ/δ ratio in Ne IX and Ne X ions). Therefore, we have not used these intensity ratio measurements for temperature determinations.

From the measured ratio of the transitions $\frac{2p\text{-}1s}{3p\text{-}1s}$ for Ne X

(L-α/L-β) with a fairly constant value of 20 to 22 for the shots without the PEOS we estimated from Table II predicted ratios, the plasma temperature to be in the 100-130 eV range when the electron density remains in the range 3 10^{21}-10^{22} cm^{-3} (see below). This corroborates the temperature estimates derived from the Ne X β/γ line ratio.

From this preliminary analysis, the inhomogeneous character of the plasma already emerges with the picture that radiation from the hydrogen-like ions originates from regions at higher temperature than the regions responsible for the helium-like radiation. Clearly, these temperature spatial gradients could be correlated to temporal gradients, the peak emission occurring at different times for each ion during the final implosion.

We did not derive any temperatures from the line intensity ratios measured for the spectra obtained from shots with the PEOS. The 3p-1s transitions often are too weak and uncorrelated to the 2p-1s line intensity to be analyzed. It seems that, in the discharges with the PEOS, the shorter duration plasma emission, as well as the slightly lower densities, (see below) enhance the non-stationary character of the imploding plasma. However, the trend towards smaller values for the α/β line ratios (~3) indicates slightly higher temperatures than in the shots without the switch, the Ne X ions emitting from regions closer to 150 eV.

We recall that the ion relaxation time (defined as the time to establish a steady-state population of the ion ground state) can be estimated, for an hydrogen-like ion such as Ne X, in the collisional radiative model of partly non-stationary plasmas (7), the model accounting for temporal changes in the particle densities. Making use of Drawin's tabulation of relaxation times (8) we note that, for a temperature around 100 eV and an electron density of 10^{21}

cm^{-3}, the ground state stationary population of Ne X ions will be reached in about 300 nsec. This relaxation time will be of the order of the plasma lifetime (~20 nsec) for a temperature around 115 eV and an electron density around 5.10^{21} cm^{-3}.

Since we have estimated the ionic velocities near the time of full implosion to be of the order of 5.10^{7} cm/sec (see Section III), a variation in electronic density by a factor of 5 (above 10^{21} cm^{-3}) will occur in ~3 nsec for a 3 mm radius plasma being further pinched at this velocity.

It is thus conceivable that, a steady-state population of the ion ground levels could be reached only very marginally at the end of the radiation duration, a situation where the use of any time-independent model to describe the plasma is highly questionable.

B. Density Estimates

The Coulomb interaction that bounds the nucleus to the excited electron in an emitting ion, may be screened by the surrounding ions and free electrons in a dense plasma. A major perturbation caused by this screening and, since long recognized (Debye and Hückel 1923) is the lowering of the ionization limit and the cutoff of the number of bound states. We observed in our neon spectra, a clear advance of the 1s-np series limit for both Ne IX and Ne X ions with the highest lying ion state corresponding to n=7 or n=6. This is displayed in Fig. 3 where the measured ionization potentials perturbed by ionic or electronic pressure are indicated. Two spectral traces are shown for a shot generated with the PEOS at two different locations along the plasma column. (Figs. 3a and 3b) Fig. 3c corresponds to a shot without the PEOS and also without spatial resolution. In these traces, the last members of the Ne IX series are shown with the measured limit at the indicated energy i.e.,

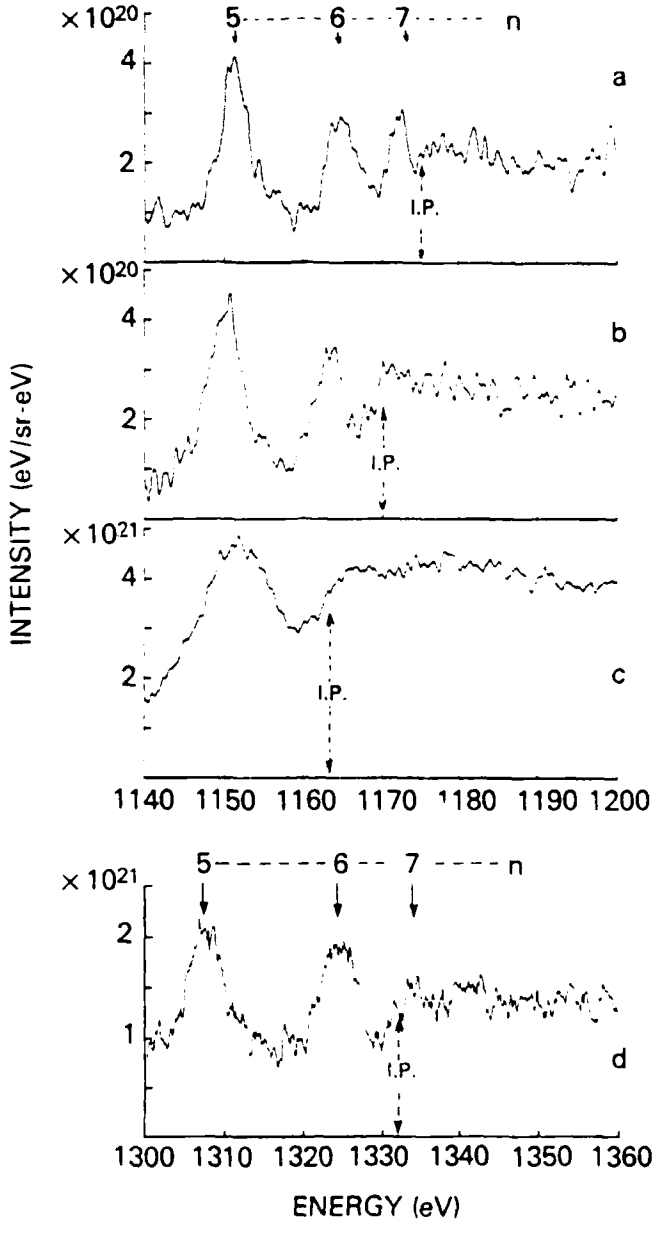

Figure 3. Spectral traces around Ne IX series limit (a-b-c) and Ne X series limit (d) showing onset of recombination continuum at the indicated ionization potential (I.P.)

a. from plasma region 1 cm away from nozzle } shot with the PEOS

b. from plasma region 2 cm away from nozzle }

c. from the whole plasma (no spatial resolution) } shots without PEOS

d. from plasma region 1 cm away from nozzle }

lower than the unperturbed limit of 1196 eV. Fig. 3d corresponds to a shot without the PEOS, but with spatial resolution and presents the last members of the Ne X series with the measured limit at an energy lower than the unperturbed limit of 1362 eV. The measured lowering of the ionization limit (ΔE) varies from 20 to 30 eV for both ion series depending on the shot and on the location along the plasma column. The accuracy of the observed ionization-limit measurements is $\pm$ 2 eV for shots with a low intensity continuum (e.g., Figs. 3a-3b) and is slightly better for the shots in Figs. 3c and 3d. Measured values for ΔE expressed in eV are tabulated in Table III for a few shots with or without the PEOS.

Note that, despite the observed line large widths (Fig. 3c) the continuum onset cannot be accounted for by the merging of broadened levels (electronic pressure) as in the standard interpretation (9) since the main contribution to the line widths is not density related (see III). Therefore, when the continuum onset is measurable as an intensity step it is not due to the merging of weak lines.

The most complete formulation of the lowering of the ionization potential of a radiating ion by the field of neighboring ions and electrons has been proposed by Stewart and Pyatt (10). They consider time-averaged charge distributions around the nucleus according to Thomas-Fermi-Dirac statistics for the electrons and a Maxwell-Boltzmann distribution for the ions; both the ion sphere and the Debye-Hückel results appear as limiting cases. Using these authors' derivation in the plasma region where the free-electron density is much larger than the ion (hence bound electron) density, the reduction in the ionization potential is written:

$$\Delta E_{ev} = -\frac{kT}{2(Z^* + 1)} \left[\left[\left(\frac{R_0}{D} \right)^3 + 1 \right]^{2/3} - 1 \right]$$

Table III

Plasma electron density from lowering of the ionization potential.

shot #	ion	plasma location	ΔE (observed) eV	N_e $x10^{21}cm^{-3}$
2531	Ne IX	cathode	26	6
	Ne X		27	6
2585*	Ne IX	along plasma length	21-26	3-6
	Ne X		25	4
2593*	Ne IX	cathode	23	4
2868	Ne IX	spatially-integrated	30	~10
	Ne X		30	8
2870	Ne IX	spatially-integrated	31	~10

*Shots obtained with the PEOS.

where Z^* is the average charge of the plasma (we shall use here $Z^* = 8.7$ for our neon plasma in agreement with the relative ionic populations derived in Table VI), R_o is the ion sphere radius, and D is the Debye length (or radius).

It is usually considered that the Debye-Huckel approximation is valid in a region where $\left(\frac{R_o}{D}\right)^3$ is small so that:

$$\Delta E \simeq \frac{Z_i}{D} e^2 \qquad Z_i \text{ ion net charge}$$

while in the region where $\left(\frac{R_o}{D}\right)^3$ is large the ion-sphere model is preferred which gives:

$$\Delta E = \frac{3}{2} \cdot Z_i \cdot \frac{e^2}{R_o}$$

Applying the usual definition of the Debye length (when both electron and

ion shielding are taken into account): $D^2 = \frac{kT}{4\pi e^2} \cdot \frac{1}{N_e + \Sigma N_i Z_i^2}$, to our plasma, we find:

$$D^2 = 55.26 \times 10^4 \cdot T \cdot \frac{1}{N_e(1+8.7)} \quad \text{and} \quad D \simeq 239 \sqrt{\frac{T}{N_e}}$$

Similarly for the neon plasma considered, the ion-sphere radius is given by:

$$R_o^3 = \frac{Zi}{4/3\pi N_e}, \text{ and } R_o = 1.25\ N_e^{-1/3}$$

Table IV gives values of R_o and D for relevant plasma parameters, T and N_e.

Table IV

N_e cm^{-3}	R_o Å	D(Å) 80	100	120	150	Te(eV)
10^{20}	27	21	23.5	26	29	
5.10^{20}	16	9.6	10.7	11.7	13.1	
10^{21}	13	7	7.5	8	9	
5.10^{21}	7	3	3.3	3.7	4.1	
10^{22}	6	2	2	2.6	2.9	

Note that the atomic matrix element $\langle r_n \rangle$ for the np orbit of the Ne X (hydrogenic) ion is, in cm: $\langle r_n \rangle = 2.645 \cdot 10^{-10}\ (3n^2-2)$
For n=6 we calculate: $\langle r_6 \rangle = 2.8 \times 10^{-8}$ cm

Noting that, for an electron density of 5.10^{21} cm^{-3} the ratio $\left(\frac{R_o}{D}\right)^3$ becomes of the order of 10, we shall start the derivation by using the ion sphere model, thus excluding a preliminary estimate of the plasma temperature (considered in equilibrium for ions and electrons in the Debye's model). The ion sphere approximation should be consistent with the derived density. It yields:

$$\Delta E_{eV} = 3/2\ e^2 \cdot Z_i^{2/3}\ (4/3\pi N_e)^{1/3}$$

which gives:

$$\Delta E = 15.10^{-7}\ N_e^{1/3} \text{ for Ne X ions}$$

$$\Delta E = 14.10^{-7}\ N_e^{1/3} \text{ for Ne IX ions}$$

Using this approximation, we have estimated the plasma electron density N_e corresponding to the measured ΔE values tabulated in Table III. The densities are listed in the last column with $\pm$ 20% uncertainty (within the plasma ion sphere model) due to our measurement accuracy.

Despite the limited accuracy of this density diagnostic which relies on the electron field statistical model, we conclude that large densities are attained at the time of radiation by both neon ions. For shots without the PEOS the electron density reaches values of the order of 6 to 10×10^{21} cm^{-3} while slightly lower values of 4 to 5×10^{21} result for shots with the PEOS.

To this range of electron densities correspond ionic densities of the order of $\frac{N_e}{Z^*}$ and average ionic distance in the plasma $(4/3\pi N_i)^{-1/3}$ of the order of 5 to 10 Å, that is not much larger than the atomic matrix element $\langle r_6 \rangle$ calculated above. A cut-off of the ion Rydberg states can thus be expected around n=6 through the process of pressure ionization.

The spectral traces in Figs. 3a and 3b emphasize this dependence of the most excited level on the plasma field, the level with n=7 disappearing in a plasma region (3b) of higher density. Despite our absolute measurement limited accuracy it is clear, from the comparison of traces in Fig. 3a and Fig. 3b, that the n=7 level characteristic evolution corresponds to a variation in electron density by a factor of 2 between two plasma regions separated by only 1 cm.

The mass loading conditions for neon implosions were discussed in Ref. 1. We shall only recall here that for shots without the PEOS, the gas-puff load at optimum pressure for maximum K-shell emission corresponds to 1.2×10^{18}

neon atoms per cm while for shots with the PEOS, there are 0.75×10^{18} neon atoms per cm. Taking the average ionic charge in the plasma $Z^* \simeq 8.7$, we obtain for both types of discharge a neon plasma diameter of only about 1/2 mm, in order to account for the derived densities. The plasma region emitting recombination continum is therefore quite pinched on the axis; it appears reasonably uniform along the plasma length in the shots with the PEOS while it is limited to the cathode vicinity in the shots without the PEOS.

If we ascribed the large densities derived to the densest spots were the NeX ions and bare nuclei predominate, our values are not too conflicting with the lower ones predicted by current modeling of gas implosions (11),(12) [2×10^{21} and $2 \times 10^{20} cm^{-3}$ respectively] since these models consider a uniform plasma column. The plasma diameters measured from time-integrated pin-hole pictures disagree also with the above conclusion but they clearly represent upper limits and do not emphasize, due to overexposure, the regions with major contribution to the radiation.

III. PLASMA SIZE AND MOTION

We discuss in the Appendix an "instrumental" source of line broadening related to spectral imaging through a convex crystal of a plasma source with finite diameter. We now consider the source of line broadening inherent in the plasma thermodynamic and dynamic properties.

For the most intense Ne IX and Ne X lines we measured line widths from the reduced line profiles for a shot without and a shot with the PEOS. Table V lists full widths at half maximum (FWHM) measured at three positions along each spectral line corresponding to three locations (C,B,A) along the plasma axis (indicated in Table V).

The large line widths observed (often of the order of 0.1 Å in some shots) cannot be accounted for by thermal Doppler broadening or by collision broadening (ion Coulomb collisions). The first mechanism would lead to plasma temperatures in the keV range and the second to electron densities in excess of $10^{22} cm^{-3}$ (13).

We note from the line width list (Table V) that, for a given location in the plasma, the α and β lines do not differ greatly in width; this rules out a large broadening contribution due to opacity. In fact, the latter could be much less than expected from a dense plasma since the radiation transfer between radially moving ions, would involve photons of different frequencies. In fact a theory developed by Irons (14) shows that the line total intensity may approach the optically thin value at sufficiently high streaming velocities. In gas-jet implosions the macroscopic radial motion of ions pinching radially during the time of x-ray emission appears as a major source of Doppler-shifts responsible for broader asymmetrical line shapes.

Table V

Observed FWHM, $\Delta\lambda$, in Å of Ne IX and Ne X lines

	plasma region	He-α	He-β	L-α	L-β
without PEOS	C	0.08	0.08	0.068	0.06
	B	0.10	~0.10	0.08	0.08
	A	0.10	0.09	~0.1	0.08
with PEOS	C	0.045	0.044	0.034	0.027
	B	0.047		0.033	
	A	0.056	0.040	0.026	0.028

C cathode region (adjacent)

B mid-gap (1.7 cm from cathode)

A near anode (~3 cm from cathode)

The observed increase in width from cathode to anode in the shots without the PEOS should be ascribed to the plasma size contribution (see Appendix) since the source diameter increases from cathode to anode in these shots. In most spectra and for both types of shots we observe a larger width for the Ne IX lines than for the Ne X lines.

From the above observations the line widths from neon plasmas may be interpreted as resulting from two major contributions: the ion radial motion (Doppler shift) and the instrumental imaging of the plasma diameter. Since both contributions are likely to be of the same order, in most shots, one needs to derive the resulting line profile from the convolution, for each thin shell of plasma, of the azimuthal contribution (expressed in terms of the

velocity component along the direction of observation) with the associated wavelength at each radial position, followed by summation of the various contributions. To perform such a computation we used the following representations: the elementary line profile was taken as Gaussian with a FWHM of 0.02 Å from KAP rocking-curve width and other plasma broadening process (Coulomb collisions essentially) considerations. Also we adopted the relationship $V(r)=V_o \frac{r}{r_o}$ between the ion radial velocity V(r) and the plasma radius r. Finally, we need to define the maximum plasma radius r_o, for ions with maximum velocity V_o, and the minimum radius r_m, the recorded radiation corresponding, with this model, to this annulus. The quantities r_o, r_m and V_o are treated as adjustable parameters and thus cannot be determined accurately. Also because of the arbitrariness in the elementary profile width, the comparison between our computed line profiles and the observed ones, allows us only to estimate the range of plasma size and ion velocity.

Examples of computed profiles for the He-α and L-α lines, according to this model, are shown in Fig. 4. The parameter values chosen are indicated. One feature of interest, in such derived profiles, is the "split", i.e., two closely-lying peaks in the line, (Fig. 4a) associated with a minimum radius $r_m \neq o$ (that is a not-fully imploded plasma). This is indeed observed in some shots. However, as emphasized in Fig. 4a, this splitting may be correlated either to a not-fully imploded plasma of .2 cm inner diameter ($2r_m$=0.2) or, to a thin plasma shell collapsing on axis with a 5.10^7 cm/s velocity. From observations on a number of shots, the evidence for two narrow-width well-resolved peaks is a good indication of the plasma radial motion. This conclusion is also based on more accurate fitting of the profile to the observed line shape.

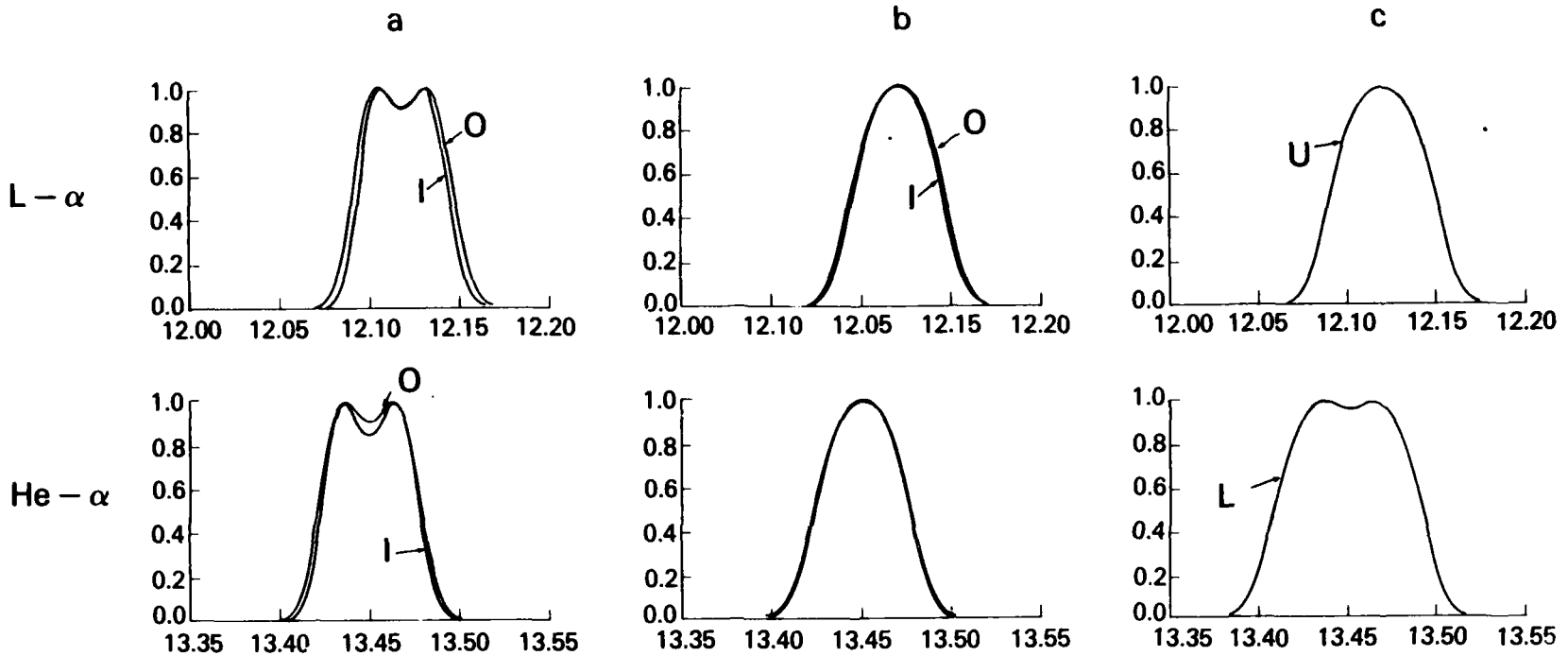

O: $V_o = 0$ $\begin{bmatrix} r_o = 0.2 \\ r_m = 0.1 \end{bmatrix}$ O: $V_o = 5.10^7$ $\begin{bmatrix} r_o = 0.15 \\ r_m = 0 \end{bmatrix}$ U: $V_o = 5.10^7$ $\begin{bmatrix} r_o = 0.2 \\ r_m = 0 \end{bmatrix}$

I: $V_o = 5.10^7$ I: $V_o = 3.10^7$ $\begin{bmatrix} r_o = 0.2 \\ r_m = 0 \end{bmatrix}$ L: $V_o = 7.10^7$ $\begin{bmatrix} r_o = 0.25 \\ r_m = 0.05 \end{bmatrix}$

Figure 4 - Computed profiles at λ_o=12.13 and 13.45 Å (L-α and He-α).

Values for the adjustable parameters are given in cm/s and cm units.

Because of the similarity of the derived profiles from both potential sources of broadening, it is not possible to determine quantitatively both the plasma radius and the ion velocity. Another example is displayed in Fig. 4b where similar profiles result from either a 3 mm diameter plasma imploding at 5×10^7 cm/s or a 4 mm diameter plasma imploding at 3×10^7 cm/s. The comparison of theoretical and experimental profiles indicates that the large line width observed in the shots without the switch should be ascribed to a not-fully imploded plasma that is an x-ray emission from ions located in an annulus with outer diameter of at least 5 mm (Fig. 4c) and inner diameter of the order of 1 mm; in this annulus the maximum velocities (at r_o) appear in excess of $5 \cdot 10^7$ cm/s for the Ne IX ions. For the Ne X ions, the velocities remain close to $5 \cdot 10^7$ cm/s and the plasma diameter below 5 mm.

In the shots with the PEOS, the plasma is more imploded at the time of emission, in particular the Ne X ions are confined to columns of maximum 2 mm diameter with velocities of the order of 3×10^7 cm/s.

Thus, the time of maximum emission appears different for each ion, the more energetic ions lying closer to the discharge axis. The ion velocity upper values derived here are clearly too large by at least a factor of 2 leading to inconsistency with the plasma internal energy value and also disagreement with the model predictions (11),(12). Improved experimental data on line widths are in need for better interpretation.

IV. ABSOLUTE SPECTRAL LINE INTENSITIES AND IONIC POPULATIONS

We have proposed, in the preceding sections estimates for the plasma temperature and electronic density based on spectroscopic diagnostics which do not rely on absolute line intensity measurements. The latter could, in principle, yield estimates of the emitting ion population using the former independent estimates for the plasma temperature and density values.

We give in Table VI the measured absolute line intensities in eV for He-α and L-α. These values are derived from three densitometer scans of a spectrum obtained from a shot without the PEOS; each scan corresponds to a plasma length of about 17% of the total as indicated in the Table first column. For a shot with the PEOS we give an average value for the measured α line intensities, the intensity variations along the plasma length being not representative within the shot-to-shot reproducibility.

Table VI

Relative populations of Ne IX and Ne X ions and Radiative time

	Radiation Source	Energy Radiated		Radiative time	Relative population	
		He-α $\times 10^{21}$	L-α eV	ns	Ne IX %	Ne X %
no PEOS	0.6 cm long near cathode	0.6	1	16	68	24
	0.6 cm long mid-gap	0.62	0.5	16	84	14
	0.6 cm long near anode	0.55	0.27	16	92	8
with PEOS	for whole plasma	2	3	12	36	51

Following the previous discussion on collisional excitation of the n=2 levels of both ions, we shall attempt to derive ion ground level populations according to equation (1). We write for the α-line radiated intensities per sec:

$$I(\alpha) = h\nu_{\alpha} \cdot Ne \cdot n_i \cdot \langle \sigma_{1-2} \cdot v \rangle$$

For the plasma electronic density N_e, we take the value obtained from the lowering of the recombination continuum onset, that is for the shots without the PEOS an estimated average of:

$$N_e \sim 8.10^{21} \text{ cm}^{-3}$$

Considering first the cathode region with n_i neon ions Ne X emitting during Δt sec and n'_i neon ions Ne IX during $\Delta t'$ sec we obtained, after expressing the collisional excitation rates $\langle \sigma \cdot v \rangle$ at an electron temperature of ~125 eV for Ne X excitation (to the n=2 level) and of ~100 eV for Ne IX excitation:

$$I\ (L\alpha) = 24.5\ 10^{10}\ n_i\ \Delta t$$

$$I\ (He\alpha) = 5.2\ 10^{10}\ n'_i\ \Delta t' \qquad (2)$$

with the line intensities I in eV.

Using the measured line intensities given in Table VI we obtain in the cathode region:

$$\begin{cases} n_i\ \Delta t = 3.9 \times 10^9 \\ n'_i\ \Delta t' = 11 \times 10^9 \end{cases}$$

Recalling that for shots without the PEOS there are about 1.2×10^{18} neon atoms per cm of column (see p. 15) and assuming that most puffed atoms reach Ne IX, Ne X or bare nucleus stage we write approximately:

$$n_i + n'_i + n_{nucl} \sim 10^{18} \text{ per cm}$$

We need an independent estimate of the relative bare nucleus population; it was obtained from the observed intensity ratio of the γ transitions assuming for each ion that the n=4 level is in thermodynamic equilibrium with

the next ion ground level. The ratio variation from 1 to 2, from cathode to anode, is thus directly interpreted as a variation of the relative population of Ne X ions to bare nuclei from 3 to 6. A similar result is obtained from the observed ratio of the β transitions (n=3). We thus, allow for a population of bare nuclei of about 30% of the Ne X ions in the cathode region and 15% or less in the other plasma regions.

With comparable radiative times for both ions, the above equations yield estimates for n_i, n'_i and $\Delta t \sim \Delta t'$. The derived relative populations and radiative times are indicated in Table VI. We note that, the 16 ns radiation time derived is not conflicting with the spectrally and spatially integrated (along the plasma length) x-ray diode (XRD) signals recording K-shell radiation pulses of the order of 30 nsec half-width for shots without the PEOS (15).

The same derivation was used to obtain the ion populations in the other regions of the plasma (Table VI). Also, for one shot without imaging slit, the Ne X population was derived from the measured Lβ intensity and found to be also around 15% for a radiation time of about 16 nsec. For the shot with the PEOS the fractional ion abundances were derived for the whole plasma (Table VI) using for the electron density an estimated value of $4.10^{21}cm^{-3}$ (Table III). However, the temperature estimate was less supported by experimental evidence (see p. 9) so that we introduced, with some arbitrariness, a value of T_e~130 eV for excitation of the Ne IX as well as Ne X levels. The total number of neon atoms was taken as $2.4x10^{18}$.

The picture that emerges from this interpretation of the absolute line intensity distribution in neon implosions is the predominance of the Ne IX ions in the plasmas generated without the PEOS. The Ne X ion population reaches only about 25% near the cathode where the ions appear to be confined.

In contrast, the much larger Ne X abundance (~50%) along the plasmas generated with the PEOS reflects a better and faster implosion. The shorter radiation time obtained from time-integrated spectral intensities agrees with the K-shell radiation narrower pulse recorded with the XRD for these shots.

The previous derivation which yields the fractional abundance estimates indicated in Table VI relies, for the plasmas generated without the switch, on the original assumption that there exists a temperature difference between the regions (and/or times) of maximum emission for both ions. We have shown that this assumption was supported by the observed line intensity ratios. It also appears necessary to reach a realistic value for the derived relative ion population ρ according to the predicted values for $\frac{R}{\rho}$ (Fig. 2). From these plotted values, we observe that a temperature difference of about 20-25 eV between both ions corresponds to a value around 0.3 for $\frac{R}{\rho}$ (and thus the population estimates in Table VI) while a common temperature for both ions, consistent with the observed Ne IX line ratios, would clearly give a much too small ρ value (~0.6) for this plasma temperature.

On the contrary, for the plasmas generated with the PEOS, lack of experimental evidence to support the assumption of temperature gradients, does yield smaller values for ρ (0.6-0.75), thus imposing a consistent plasma model with a common higher temperature for both ions.

V. SUMMARY

The simple analysis that we suggested to describe the Ne IX and Ne X α transitions that dominate the neon plasma emission, accounts for the observed line intensity variations without any further assumption on temperature variation along the plasma other than the initial one of a difference between the Ne IX and Ne X emission regions in the plasmas generated without the switch. For the shots with the PEOS, although the average plasma temperature

appears higher, an attempt to derive it from spectroscopic measurements is not easy at this time, considering the apparent larger departure from ionization equilibrium as well as the lower available intensities.

However, from our basic experimental observations we were able to characterize our neon plasmas in terms of:

- electron temperature range: 100-140 eV
- electron density range: $5\text{-}8.10^{21}$ cm^{-3}
- ion velocity upper limit: 5.10^{7} cm/s
- uniformity: variations in line intensities by a factor of 2 to 4 in shots without the switch, negligible in shots with the PEOS.

Although time-resolved data are needed for any discussion of basic processes in plasma formation, the space-resolved but time-integrated results suggest that temperature/density variations exist along the plasma as well as non-uniform ionic populations. A better uniformity is observed in the plasmas generated with the PEOS, in agreement with the other diagnostic conclusions. Nevertheless, due to the very nature of imploding plasmas, fast local variations of T_e (heating) and N_e (heating and compression) occur, leading to non-steady ionic populations and departure from ionization equilibrium. While our spectral lines display no distinct asymmetry to discriminate between a collapsing or an expanding plasma, our data, with different line widths for both ions, seem to indicate that the beginning of intense x-ray emission occurs prior to stagnation. At this point, it is clear that more diagnostics, in particular the spectral line time--history, are needed to shed light on the important topic of plasma hydrodynamic and atomic modeling.

In this report, most of our data interpretation focused on absolute line intensity measurements but work is still in progress to interpret our line profiles. In particular we shall attempt to correlate the observed line-shape

spatial variation along the interelectrode gap with the so-called "zipper-effect" described in imploding gas experiments (16) (17).

ACKNOWLEDGEMENTS

The authors wish to acknowledge helpful discussions with S. Stephanakis, F. Young, J. Apruzese and J. Davis. Constructive comments on the manuscript by F. Young, G. Doschek, and J. Apruzese were appreciated. One of the authors (P.G.B.) is appreciative of the help of R. D. Cowan of LANL for the use of his atomic structure program. D. J. Nagel's continuous interest in this work was appreciated. This research was supported in part by the Defense Nuclear Agency.

Appendix

Geometrical Broadening of a spectral line associated with a finite source size

The "instrumental" width of spectral lines from plasmas with finite radius r_p are computed here for our particular spectrograph, a convex crystal viewing the whole plasma diameter. The derivation is done for the practical geometry with a source-to-crystal distance L much larger than the plasma radius ($L \gg r_p$).

Rays from two points P, P' in the plasma can therefore be diffracted at two different locations S, S' on the film for the same wavelength λ (same Bragg angle θ).

Illustrating this effect (with a non-realistic scale) in Figure I we consider the ray originating in P, incident at point A (on crystal) as the x axis. With our geometry, this ray is perpendicular to OO', the z axis, O being the crystal axis intersection with the incident plane, O' that of the film cylinder with the same plane. The Bragg angle θ at point A (Fig. I) is thus simply equal to ω for the ray from the source center. We shall use this simplification in the final derivation.

Figure I

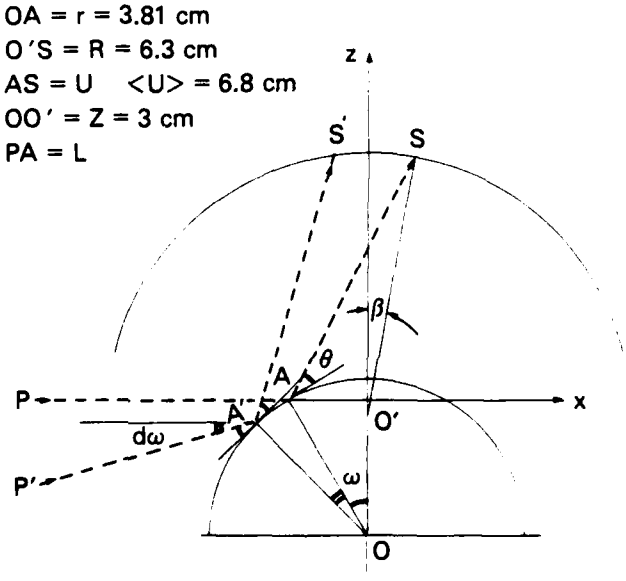

Since we want to calculate the distance SS' = ds on the film with ds = $Rd\beta$ (R film radius) we begin by expressing the vector $\vec{AS}$ as a function of the angle β. The magnitude $\cup$ of $\vec{AS}$ can be computed separately and will be taken as constant over our spectral range and with a KAP crystal.

Projecting $\vec{AS}$ on both axis gives two relations:

$$\begin{cases} \cup \sin(\theta+\omega) = R\cos\beta - r.\cos\omega + Z \\ \cup \cos(\theta+\omega) = -R\sin\beta + r.\sin\omega \end{cases}$$

with Z = 00'

Eliminating $\cup$ we obtain the relation between β and ω for any Bragg angle θ:

$$\sin(\theta+\omega)\,(r\sin\theta - R\sin\beta) = \cos(\theta+\omega)\,(R\cos\beta - r\cos\omega + Z)$$

When the incident ray makes an angle $d\omega$ (small) with the x axis as shown in Fig. 1 at point A' (not at scale) the angle β changes by the amount $d\beta$ according to:

$$Rd\beta\cdot\sin(\theta+\omega-\beta) = d\omega\left[Z\sin(\theta+\omega) + R\sin(\theta+\omega-\beta)\right].$$

We may now use the experimental relation $\omega=\theta$ with $ds=Rd\beta$ to obtain:

$$ds = d\omega\left[R + \frac{Z\sin 2\theta}{\sin(2\theta-\beta)}\right]$$

The angle β is obtained from: $\beta = \arcsin\left(\frac{r\sin\theta - \cup\cos 2\theta}{R}\right)$

We give below the calculated values of β, ds and $d\lambda$ using the reciprocal dispersion from the observed spectra of 1.45 Å/cm at 13 Å and 1.65 Å/cm at 10 Å. We restricted the calculations to two lines He-α and L-β which is sufficient to indicate that ds does not vary much over our spectral range.

line	λ Å	θ degrees	β	ds cm	$d\lambda$ Å
He-α	13.45	30.4	-12.74	9 $d\omega$	13.1 $d\omega$
L-β	10.24	22.64	-31.78	8.5 $d\omega$	14 $d\omega$

We need to express the angular divergence $d\omega$ in terms of the plasma radius r_p. It can be shown readily that:

$$d\omega = \frac{r_p}{L+r\sin\theta} \sim \frac{r_p}{L}$$

For most of the spectra from which we derived line widths the distanct L from source to crystal apex was about 87 cm. The spectral image breadth on each side of the center (paraxial rays) has therefore a value $d\lambda_p$ in Å of 0.15 r_p for He-α and 0.16 r_p for L-β.

The plasma diameters determined from x-ray pinhole images at 3 different locations along the plasma are given below. We mentioned on p.16 that they represent upper limits, possibly much larger than the actual plasma size.

Plasma Diameter $2r_p$ in cm

Shot #	Cathode vicinity	Middle gap	Anode region
2531	0.15	0.25	~0.3
2585	0.15	~0.2	0.2
2594	<0.1	0.2	0.2

For the longest distance used (L ~158 cm), the line breadths from center are only 0.08 r_p for He-α and 0.09 r_p for L-β.

References

(1) G. Mehlman, P.G. Burkhalter, D.A. Newman, S.J. Stephanakis, F.C. Young, and D.J. Nagel, J. Appl. Phys. 60, 3427 (1986).

(2) J.D. Garcia and J.E. Mack, J. Opt. Soc. Am. 55, 654 (1965).

(3) A.M. Ermolaev and M. Jones, J. Phys. B7, 199 (1974).

(4) R.D. Cowan, J. Opt. Soc. Am. 58, 808 (1968); R.D. Cowan and D.C. Griffin, J. Opt. Soc. Am. 66, 1010 (1976).

(5) I.I. Sobelman, L.A. Vainshtein and E.A. Yukov, Excitation of Atoms and Broadening of Spectral Lines (Springer Verlag Berlin.. 1981).

(6) R.W.P. McWhirter, Plasma Diagnostic Techniques (Acad. Press. New York, 1965) p. 206.

(7) R.W.P. McWhirter and A.G. Hearn, Proc. Phys. Soc. of London 82, 641 (1963).

(8) H.W. Drawin, J. Quant. Spectrosc. Radiation Transfer. 10, 33 (1970).

(9) D.R. Inglis and E. Teller, Astrophys. J. 90, 439 (1939).

(10) J.C. Stewart and K.D. Pyatt, Astrophys. Journ. 144, 1203 (1966).

(11) J. Davis, C. Agritellis and D. Duston, NRL Memorandum Report No. 5615, July 1985.

(12) S.W. McDonald and P.F. Ottinger, NRL Memorandum Report No. 5785, June 1986.

(13) H.R. Griem, Plasma Spectroscopy (McGraw Hill New York) (1964).

(14) F.E. Irons, J. Phys. B9, 2737 (1976).

(15) S.J. Stephanakis, J.P. Apruzese, P.G. Burkhalter, J. Davis, R.A. Meger, S.W. McDonald, G. Mehlman, P.F. Ottinger and F.C. Young, Appl. Phys. Lett., 48, 829 (1986).

(16) W. Clark, R. Richardson, J. Brannon, M. Wilkinson and J. Katzenstein, J. Appl. Phys. 53, 5552 (1982).

(17) S.J. Stephanakis, J.R. Boller, D.D. Hinshelwood, S.W. McDonald, G. Mehlman, P.F. Ottinger, F.C. Young, Record.-Abstr. 1985 IEEE Inter. Conf. Plasma Sci., Pittsburgh, 1985, p. 55.

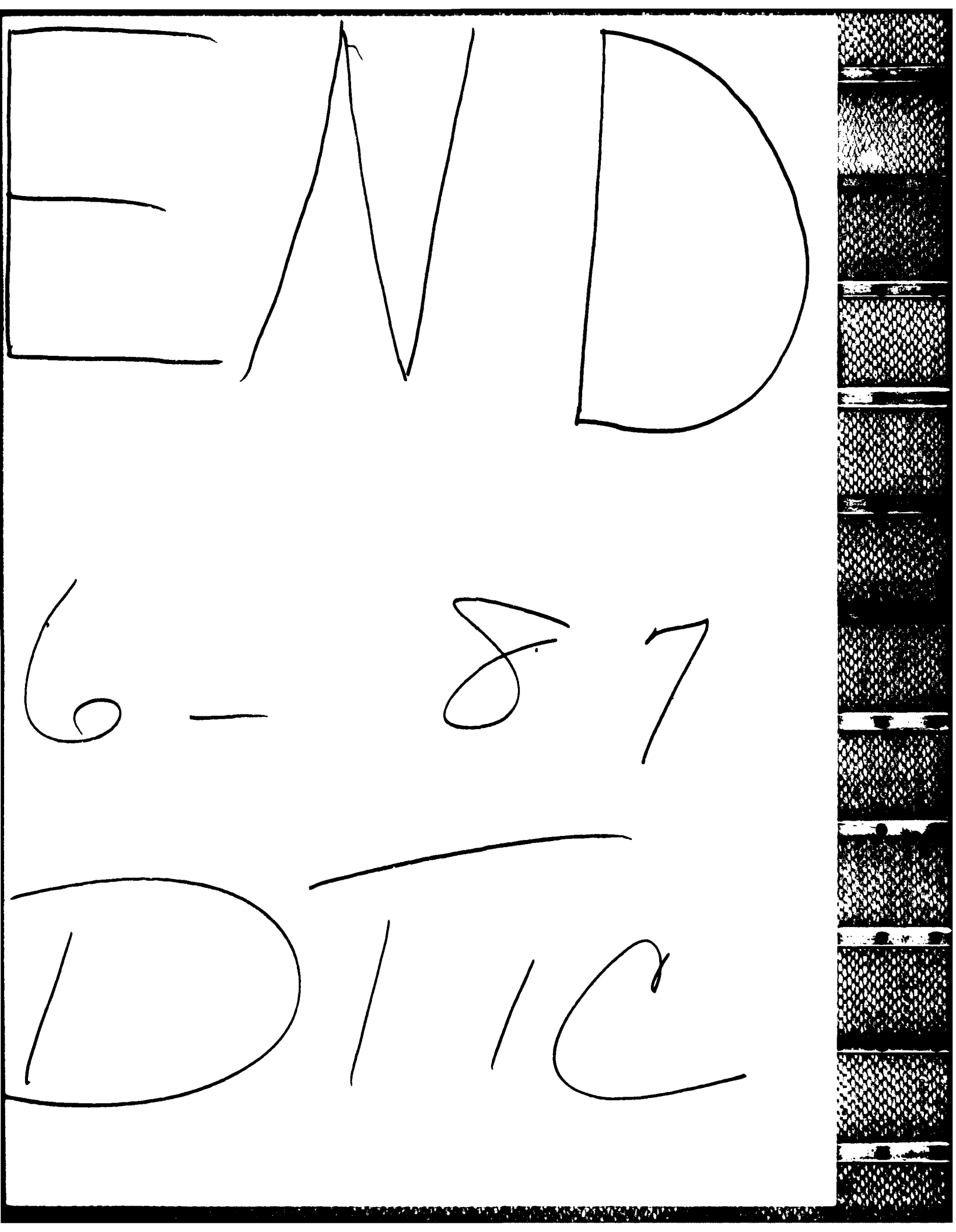
END
6-87
DTIC